



Enhanced UV-light driven photocatalytic performance of magnetic $\text{CoFe}_2\text{O}_4/\text{TiO}_2$ nanohybrid for environmental applications

Samuel Brito Ferreira Santos¹ · Luana Rabelo Hollanda¹ · Yasmin Vieira² · Guilherme Luiz Dotto^{2,3} · Edson Luiz Foletto² · Osvaldo Chivone-Filho¹

Received: 10 October 2022 / Accepted: 15 May 2023 / Published online: 22 May 2023
© The Author(s), under exclusive licence to Springer-Verlag GmbH Germany, part of Springer Nature 2023

Abstract

In this work, $\text{CoFe}_2\text{O}_4/\text{TiO}_2$ nanostructure was prepared through a facile and effective solvothermal route for efficient use in the degradation of the Erionyl Red A-3G model pollutant under ultraviolet irradiation. Characterization analysis indicated the successful heterojunction among the precursors. The composite presented band gap value of 2.75 eV, being smaller than that of the pristine TiO_2 , as well as mesoporous structure. The catalytic activity of nanostructure was investigated by employing a 2^2 factorial experimental design with 3 central points. The optimized reaction conditions were set as $\text{pH} = 2$ and catalyst dosage = 1.0 g L^{-1} for an initial pollutant concentration of 20 mg L^{-1} . The prepared nanohybrid presented remarkable catalytic activity, reaching color removal efficiency of 95.39% after 15 min, as well as total organic carbon (TOC) removal of 69.4% after 120 min. The kinetic studies of TOC removal followed the pseudo-first order model, with a rate constant of 0.10 min^{-1} . Moreover, the nanostructure presented magnetic behavior, being easily separated from the aqueous medium through the use of a simple external magnetic field.

Keywords $\text{CoFe}_2\text{O}_4/\text{TiO}_2$ · Photocatalysis · Erionyl Red · Experimental design · Kinetic

Introduction

Advanced oxidation processes are promising technologies proposed for the complete degradation of organic pollutants through the generation of highly reactive free radicals capable of oxidizing various stable molecular structures (Hollanda et al. 2021). Within the various advanced oxidation processes, heterogeneous photocatalysis stands out due to the coupling of oxidation and reduction reactions induced by the application of light irradiation to the surface of semiconductor materials without the need for adding any precipitating agent to remove the solid catalyst (Vieira et al. 2019).

Over the years, titanium dioxide (TiO_2) has been the most explored catalyst for heterogeneous photocatalysis, widely used due to its high photocatalytic efficiency under ultraviolet light (Lazarotto et al. 2020; Silvestri et al. 2020). However, even though TiO_2 constitutes a heterogeneous phase with water, the difficulty in recovering this material at the end of the reaction constitutes a challenge for its use on a commercial scale (Vaiano et al. 2020).

Thus, even though these technologies have been developed and improved over the last 20 years, several operational drawbacks limit their application, such as lack of light absorption efficiency in photocatalysis, in addition to the need for several mechanical unit operations (Rossatto et al. 2020; Fuziki et al. 2021). In this context, coupling two or more semiconductors is proposed as a compelling alternative, since it reduces the band gap value, allowing a more effective reaction conversion without the need for using highly energetic light sources. Moreover, semiconductors can improve electron mobility and reduce electron-hole combinations. Thus, it becomes obvious that increasing the overall efficiency can decrease the overall process time, thereby reducing operational costs (Oseghe and Ofomaja 2018; Vieira et al. 2022).

Responsible Editor: Philippe Garrigues

✉ Guilherme Luiz Dotto
guilherme_dotto@yahoo.com.br

¹ Department of Chemical Engineering, Federal University of Rio Grande do Norte, Natal 59078-970, Brazil

² Department of Chemistry, Federal University of Santa Maria, Santa Maria 97105-900, Brazil

³ Department of Chemical Engineering, Federal University of Santa Maria, Santa Maria 97105-900, Brazil

It is possible to combine TiO_2 with other semiconductors with much smaller band gaps, such as cobalt ferrite (CoFe_2O_4), which also shows magnetic character, allowing the final catalyst obtained to be separated through the application of a simple external magnetic field (Van et al. 2021; Mapossa et al. 2021). In other words, the coupling of CoFe_2O_4 , with an approximate band gap of 1.5 eV, with TiO_2 , that presents a band gap higher than ~ 3 eV, is capable of tuning and tailoring the band gap of the synthesized hybrid phase (Ciocarlan et al. 2020; Krishna et al. 2020). Thus, the resultant material acquires an intermediate and more effective band gap for the use in photocatalysis, while also resulting in a magnetic catalyst. Heterojunction structures between TiO_2 and CoFe_2O_4 have been previously proposed as suitable photocatalysts in the degradation reactions of different organic molecules in an aqueous environment (Mourão et al. 2010; Balu et al. 2011; Sathishkumar et al. 2013).

A few works addressing degradation of different types of Erionyl dye by heterogeneous photocatalysis have been reported in the literature. For instance, phodegradation of erionyl blue dye (Acid blue 260) has been evaluated in aqueous medium by sunlight and palladium catalysts (Pérez-Osorio et al. 2019). Erionyl Red B dye (Acid Red 151) has been degraded by photocatalytic process using activated carbon/ TiO_2 composite under UV irradiation (Silva et al. 2006). TiO_2 catalyst (Degussa P25) under UV irradiation has been employed for degradation of Navy Erionyl R 180% (Zayani et al. 2006). However, to the best of our knowledge, Erionyl Red A-3G has not yet been investigated as target pollutant molecule on photocatalytic studies. Thus, $\text{CoFe}_2\text{O}_4/\text{TiO}_2$ heterojunction was selected as a photocatalyst and prepared herein for use on the degradation reaction of the respective pollutant molecule. In this work, $\text{CoFe}_2\text{O}_4/\text{TiO}_2$ nanostructure was prepared by the solvothermal route and posteriorly applied as a photocatalyst for Erionyl Red A-3G removal in an aqueous medium under ultraviolet irradiation. The catalytic activity was investigated using a 2^2 -factorial experimental design with 3 central points, where the pH and catalyst dosage were the investigated variables.

Methodology

Preparation of composite

The CoFe_2O_4 particles were obtained through the solvothermal route by mixing cobalt chloride ($\text{CoCl}_2 \cdot 6\text{H}_2\text{O}$) and iron chloride ($\text{FeCl}_3 \cdot 6\text{H}_2\text{O}$) salts at the proportion of 1:2 mmol of Co:Fe. The salts were dissolved in ethylene glycol under magnetic agitation, and 60 mmol of sodium acetate ($\text{NaC}_2\text{H}_3\text{O}_2$) was added to this solution. The mixture was transferred to a Teflon-lined stainless steel autoclave, which was kept at 200 °C for 24 h. The solids obtained were filtered, washed

with distilled water and ethanol, and air-dried for 24 h. The material was used as a precursor in the $\text{CoFe}_2\text{O}_4/\text{TiO}_2$ composite preparation, designed at 10:90 ($\text{CoFe}_2\text{O}_4:\text{TiO}_2$) mass/mass ratio. The TiO_2 used was commercially obtained. The synthetic procedure followed the same step used in preparing the precursor material (CoFe_2O_4). The $\text{CoFe}_2\text{O}_4/\text{TiO}_2$ composite obtained was named 90Ti.

Characterization techniques

X-ray diffraction analysis (XRD) was performed on a Miniflex (Rigaku) diffractometer, with $\text{Cu-K}\alpha$ radiation ($\lambda = 1,54051 \text{ \AA}$) and energy source operating at 30 kV and 10 mA. Fourier transform infrared spectroscopy (FTIR) was recorded on an IRPrestige-21 (Shimadzu) spectrometer through the transmittance recording method and KBr as a sample dispersing medium. Particle size distribution was estimated by dynamic light scattering (DLS), using colloidal Ludox TM-50 as the dispersant phase, with nanoparticle analyzer model SZ-100 (Horiba Scientific). The histograms obtained were analyzed, and the limit of detection of the method was in the range of 0.3 to 8000 nm. The textural properties were analyzed by N_2 adsorption/desorption isotherms at liquid-nitrogen temperature (77 K) using an ASAP 2020 instrument. Surface area (S_{BET}) and pore size distribution were calculated according to Brunauer, Emmett e Teller (BET), and Barrett–Joyner–Halenda (BJH) methods (Sing et al. 1985; Thommes et al. 2015). The morphology of the catalysts was investigated through scanning electron microscopy (SEM) coupled do energy dispersive spectroscopy (EDS) with a JSM 6010LV (JEOL) microscope. The band gap of the samples was calculated according to the Kubelka-Munk method (Vieira et al. 2020), with data obtained through diffuse reflectance at the ultraviolet (UV) and visible (Vis) method, using Cary 5G UV-Vis (Varian) spectrophotometer.

Photocatalytic experiments

The catalytic potential of the synthesized materials was investigated in a laboratory-scale batch system designed for photocatalysis, as shown in Fig. 1. The system consisted of an annular reactor made of borosilicate, with an approximate volume of 1 L, constructed around an encapsulated UV lamp (mercury vapor, 250 W). The reactor temperature was kept at 20 °C, enclosed by circulating and constant water flow controlled with a thermostatic bath. All the parts previously described were built inside a sealed box for entire isolation from any external light sources. The experiments consisted of a reaction volume of 400 mL at a temperature of 20 °C. The initial concentration of the target pollutant Erionyl Red A-3G (also named as Acid Red 447, CAS No. 141880-36-6; widely used in the textile industry) chosen for the experiments was fixed at 20 mg L⁻¹, whose value is within the

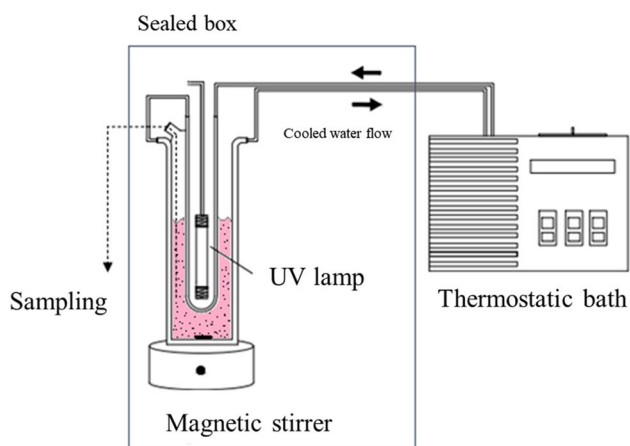


Fig. 1 Schematic representation of the laboratory scale batch system designed for the photocatalysis experiments

range of the concentration of textile dyes discarded in industrial effluents (Yaseen and Scholz 2019). The optimal pH and catalyst dosage were investigated by employing an experimental design described in the following section. Adsorption equilibrium was reached by stirring the catalyst and dye in the dark, and after, the photocatalytic reaction was started by turning on the UV lamp.

Analytical procedures

The degradation of the Erionyl Red A-3G dye solution was monitored by molecular absorption spectrometry technique on a UV–Vis spectrometer (UV-2600, Shimadzu), at the maximum absorption wavelength of 552 nm. The $R\%$ was estimated as shown in equation 1, where C_o and C are the dye concentrations at initial and t time, respectively.

$$R (\%) = \frac{C_o - C}{C_o} \cdot 100 \quad (1)$$

Total organic carbon (TOC) was measured by TOC- $L_{CPH/CPN}$ equipment (Shimadzu) for optimal experimental condition. Sample preparation consisted of filtration with PTFE syringe filters (0.22 μm , AllCrom). The TOC mineralization efficiency (%) was calculated according to equation 2, where TOC_0 and TOC stand for the TOC concentration for the initial and final sampling points during the reaction.

$$\text{TOC removal efficiency } (\%) = \left(1 - \frac{\text{TOC}}{\text{TOC}_0}\right) \cdot 100 \quad (2)$$

Experimental design

The optimized experimental conditions were found by employing a 2^2 -factorial design with triplicates at the central points, and the efficiency was estimated by setting color

Table 1 Experimental design matrix with the coded and uncoded values for X_1 (pH) and X_2 (catalyst dosage) variables and results

| Experiment | X_1 | X_2 | pH | Catalyst dosage (g L^{-1}) | $R\%$ |
|------------|-------|-------|----|---------------------------------------|-------|
| 1 | -1 | -1 | 2 | 0.1 | 25.15 |
| 2 | +1 | -1 | 4 | 0.1 | 28.79 |
| 3 | -1 | +1 | 2 | 1.0 | 95.40 |
| 4 | +1 | +1 | 4 | 1.0 | 64.72 |
| 5 | 0 | 0 | 3 | 0.55 | 76.23 |
| 6 | 0 | 0 | 3 | 0.55 | 70.77 |
| 7 | 0 | 0 | 3 | 0.55 | 69.97 |

removal efficiency ($R\%$) as the response. The two independent variables investigated were pH and catalyst dosage (g L^{-1}), coded as X_1 and X_2 . Variable X_1 ranged from 2 to 4, and X_2 ranged from 0.1 to 1.0 g L^{-1} , as presented in Table 1. Responsive surface methodology (RSM) results were interpreted with Statistica software. All models were validated, and the statistical significance of the set of linear and quadratic coefficients and their interactions were obtained by analysis of variance (ANOVA) with a 95% confidence interval ($p < 0.05$). The pH values chosen for the experimental design were determined according to the development of a set of preliminary experiments, described in detail in the next sections. Based on those results, the pH values selected were 2, 3, and 4. The catalyst dosage values were selected according to the literature, being 0.1, 0.55, and 1.0 g L^{-1} , since the range between 0.1 and 1 g L^{-1} is often employed successfully in photocatalytic reactions for the degradation of environmental pollutants (Parhizkar and Habibi 2018; Wang et al. 2021).

Results and discussion

Characterization results

Characterization results for the used samples in this work are shown in Fig. 2. From Fig. 2(a), it is possible to observe the XRD patterns for the 90Ti, TiO_2 , and CoFe_2O_4 samples. It is possible to confirm that there was the monophasic formation of CoFe_2O_4 , as it is shown by the presence of the characteristic peaks in 2θ at 18.17° , 30.23° , 36.68° , 35.24° , 43.28° , 53.21° , 56.84° , and 62.33° , as well as its respective reflection planes (111), (220), (311), (222), (400), (422), (511), and (440), matching the crystallographic record card no. JCPDF 22-1086 and other results reported in the literature (Vlazan and Stoia 2018; de Oliveira et al. 2019). The more relevant peaks which have resulted from the merging of CoFe_2O_4 and TiO_2 are highlighted for the composite 90Ti sample according to its respective precursor material, i.e., anatase phase

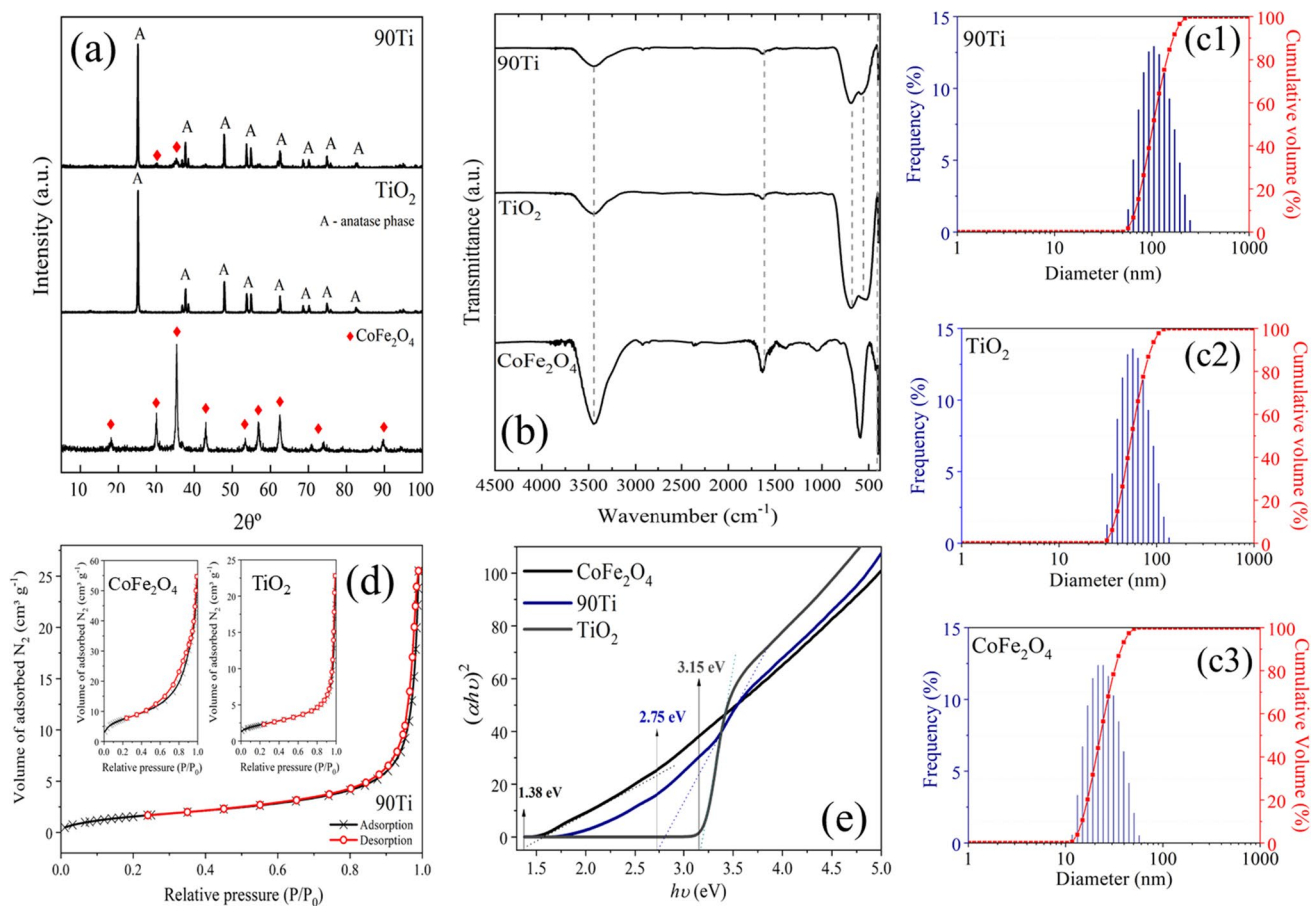


Fig. 2 **a** XRD and **(b)** FTIR patterns for the different samples. Particle size distribution histograms for **(c1)** 90Ti composite, **(c2)** TiO₂, and **(c3)** CoFe₂O₄. **(d)** N₂ adsorption–desorption isotherms for 90Ti

composite, with inserted isotherms for TiO₂ and CoFe₂O₄. **(e)** Tauc plots and band gap values for 90Ti, TiO₂, and CoFe₂O₄ samples

for TiO₂ and characteristic monophasic peaks for CoFe₂O₄, indicating that the heterojunction between powders was successful. The decrease in the relative intensity of the phase added in smaller concentration is expected for composites with two or more precursors, as it has been shown for similar composites obtained by hydrothermal and reflux condensation routes (Sun et al. 2020; Fuziki et al. 2021).

In the FTIR spectra shown in Fig. 2(b), it is demonstrated that all the samples have characteristic bands at around 3457 and 1633 cm⁻¹, which can be attributed to the stretching of –OH surface groups, possibly due to free and adsorbed water. In addition, the band at around 591 cm⁻¹ confirms the oxygen-metal stretching at tetrahedral sites, indicating the formation of metallic oxides for all samples. For the CoFe₂O₄ sample, the presence of a small peak at 429 cm⁻¹ indicates Co–O bonding at tetrahedral sites. For the 90Ti sample, however, the characteristic Co–O peak is showed by the broad band of Ti–O bonding (Sun et al. 2020). Moreover, other studies have obtained similar patterns for nanoparticle synthesis employing ethylene glycol as a synthesis medium

(Vlazan and Stoia 2018). In Fig. 2c1–c3, it is shown the samples' frequency histograms and average particle size distribution. The average particle size obtained for 90Ti, TiO₂, and CoFe₂O₄ was 102.7, 54.6, and 23.0 nm. Moreover, the dispersion behavior can be classified as monomodal, with a leptokurtic and slightly asymmetric distribution profile.

The N₂ adsorption–desorption isotherms for the 90Ti composite are presented in Fig. 2(d) and inserted given the plots for CoFe₂O₄ and TiO₂ precursors. It can be observed from the plots shown that the behavior for N₂ adsorption isotherms follows classifications II and III (Sing et al. 1985). Thus, the materials present multilayer adsorption and mesoporous structure characteristics. Moreover, the slight hysteresis loop can still be classified as H3 type, which indicates non-rigid aggregates with plate-shaped particles and slit-shaped pores. The S_{BET} for CoFe₂O₄, TiO₂, and 90Ti was calculated to be 27.20, 7.99, and 6.34 m² g⁻¹, with an average pore volume of 0.09, 0.03, and 0.04 cm³ g⁻¹, respectively.

At last, in Fig. 2(e), the Tauc plots are shown for estimating the band gap values for each material, determined

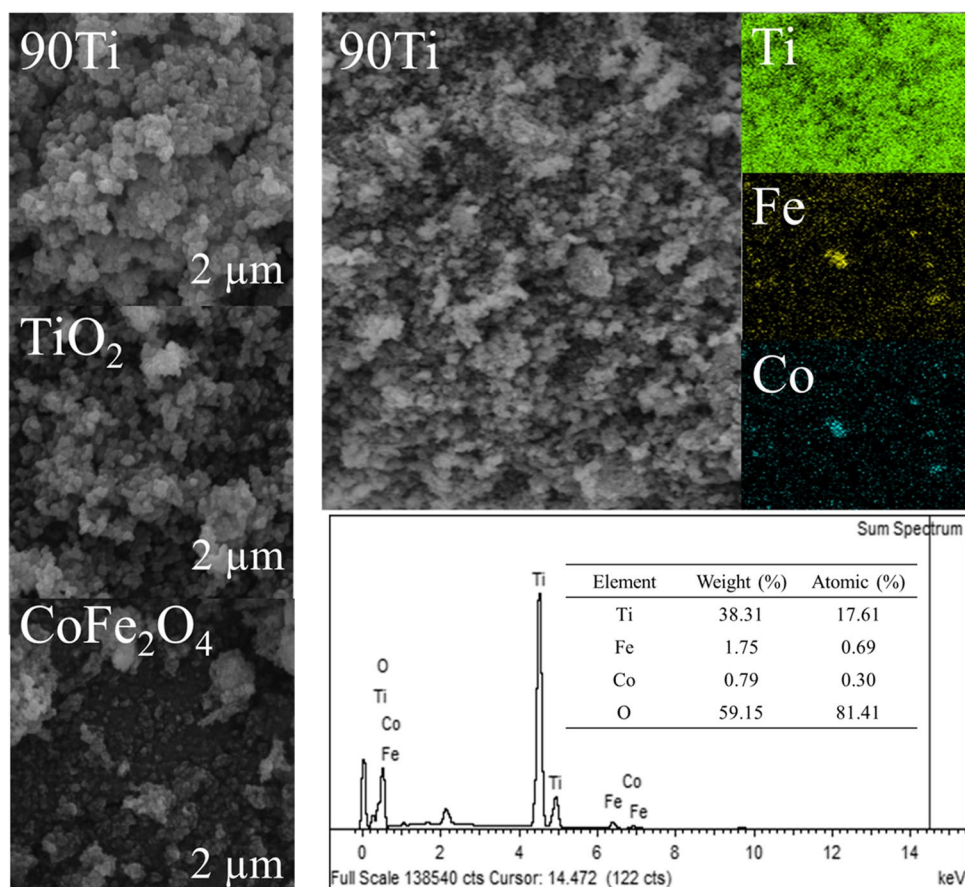
according to the Kubelka-Munk function (Vieira et al. 2022), based on the UV-Vis diffuse reflectance spectra. The band gap values estimated for CoFe_2O_4 , TiO_2 , and 90Ti were calculated to be 1.38, 3.15, and 2.75 eV, according to the extrapolation of each respective inflection point. Thus, the addition of CoFe_2O_4 , even at small proportions to TiO_2 , can result in the narrowing of the optical band gap, caused by the contribution of crystalline defects present in the TiO_2 structure (oxygen vacancy), as well as the presence of transition elements (Co, Fe) (Stefan et al. 2021). Complementarily, in Fig. S1, it is possible to observe a characteristic optical behavior for TiO_2 at the UV region, from 200 to 380 nm, limited at around 400 nm. The CoFe_2O_4 , on the other hand, exhibited optical activity over a wide wavelength range, covering both the UV and visible regions, with an absorption threshold close to the wavelength of 900 nm. At last, it is possible to see that for the 90Ti sample, an intensification of absorption in the UV region and extended optical activity to the visible region occurred, with an absorption limit for wavelengths close to 900 and 775 nm.

In Fig. 3, it is presented the SEM micrographs for the 90Ti, TiO_2 , and CoFe_2O_4 samples, and elemental mapping and EDS analysis for the 90Ti sample

particle size distribution obtained through DLS analysis, which pointed to the formation of nanosized particles. For the 90Ti sample, it is possible to see uniform clusters and roundly shaped, whose color is closer to the white color of the TiO_2 nanoparticles, added in greater proportion, with smaller dark spots and characteristic of CoFe_2O_4 nanoparticles. The morphology shown in the micrograph for CoFe_2O_4 nanoparticles is characterized by the formation of non-uniform clusters resulting from the agglomeration of the nanoparticles caused by the interfacial surface tension during the synthesis. Similar morphological results were reported by Heydari et al. (2021) and Nabi et al. (2020), which have observed the formation of irregular, semi-spherical nanoparticles, and constituting agglomerates. For TiO_2 , a predominant spherical shape with clusters was observed under the literature reports (Heydari et al. 2021; Abram and Dražić 2021).

From the elemental mapping, also shown in Fig. 3, it is possible to see a homogeneous distribution of Ti, Fe, and Co, with only a few spots concentrating more on Fe and Co over others, demonstrating the successful heterojunction between TiO_2 and CoFe_2O_4 at the 90Ti composite. In this way, the homogeneous distribution of metals over a composite sample is fundamental for photocatalytic purposes

Fig. 3 SEM micrographs for the 90Ti, TiO_2 , and CoFe_2O_4 samples, and elemental mapping and EDS analysis for the 90Ti sample



(Oliveira et al. 2016; Oliveira et al. 2018). According to the EDS analysis, the composite sample (90Ti) contains 38.31%, 1.75%, and 0.79% of Ti, Fe, and Co, respectively. The remaining sample composition can be attributed to oxygen in the oxide form. Ultimately, it is possible to infer that the $\text{CoFe}_2\text{O}_4/\text{TiO}_2$ composite was successfully obtained through the proposed solvothermal route, with very interesting properties, such as a 2.75 eV band gap, being a value smaller than that for pristine TiO_2 . The decrease in the band gap value is a very desirable trait for catalysts, especially when they are designed to be photoactivated because if energy absorption by the material occurs on longer wavelengths, it allows successful applications of the produced catalyst using less energetic regions of the electromagnetic spectrum (Silvestri and Foletto 2017; Hafeez et al. 2019). In this way, the formation of the $\text{CoFe}_2\text{O}_4/\text{TiO}_2$ heterojunction, as shown by characterization results, can enhance the separation of electronic charge flow during the reaction and reduce charge and electron-hole recombination on the surface of the material, favoring the photocatalytic process (Vieira et al. 2022).

Photocatalytic activity

Photocatalytic experiments were carried out to investigate the effects of a wider pH range using 90Ti catalyst, possible to see the results in Fig. 4. The reaction conditions were the volume of 400 mL, initial concentration of target pollutant of 20 mg L^{-1} , and catalyst dosage of 0.55 g L^{-1} . Four experiments were carried out at pH values of 2, 4, 5, and 7. From Fig. 4, it can be observed that the degradation of the contaminant occurred at greater intensity for acidic pH values ($\text{pH} < 5$). For $\text{pH} = 2$, total contaminant degradation was reached within 60 min. At $\text{pH} = 4$, the time needed for the same efficiency as for $\text{pH} = 2$ to be reached doubled, resulting in the need for 120 min of reaction. Lastly, no significant difference was reached for $\text{pH} = 5$ and 7, with maximum removal of 63% after 120 min. These results can be explained as resulting from a combination of factors, such as the fact that the target pollutant is an anionic dye that becomes negatively charged under $\text{pH} = 4$, as well as 90Ti catalyst particles, exhibit positively charged surfaces, enhancing the interaction between catalyst-pollutant by physical attraction (Oliveria et al. 2017; dos Santos et al. 2019; de Oliveira et al. 2019). Ultimately, according to the results, pH range between 2 and 4 was selected for the experimental design.

The photocatalytic results for all the investigated experimental conditions according to the factorial experimental design are shown in Table 1, expressed as $R\%$ after 15 min of reaction. The highest $R\%$ value was reached by run 3, with $\text{pH} = 2$ and catalyst dosage = 1.0 g L^{-1} . As a tendency, it is possible to observe that lower $R\%$ was reached for lower catalyst dosages were used, but pH also played an important role in the efficiency.

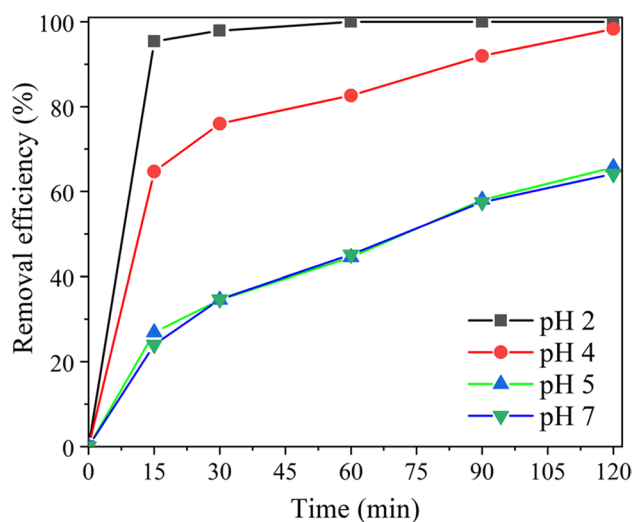


Fig. 4 Color removal ($R\%$) as a function of pH using 90Ti catalyst (reaction conditions: initial dye concentration = 20 mg L^{-1} and catalyst dosage = 0.55 g L^{-1})

The quantitative significance of the effects for the studied variables was analyzed using a Pareto diagram, shown in Fig. 5(a). The most relevant effects are caused by variable X_2 (catalyst dosage). It is also possible to observe that the effects caused by variable X_2 (catalyst dosage) exert a linear influence on the model. In contrast, variable X_1 (pH) exerts a quadratic effect, but both are significant for the $R\%$ values obtained. Moreover, the analysis of the meaning behind the positive and negative values for X_2 and X_1 shows that as the catalyst dosage increases and pH decreases, the higher the $R\%$ value. In Fig. 5(b), it is presented the response surface obtained for the experimental design. According to the model, the optimized conditions were $\text{pH} = 2$ and catalyst dosage = 1.0 g L^{-1} . The equation representing the model is given in Eq. 3, obtained with a 95% significance level and R^2 equal to 0.994.

$$R(\%) = -140.58 + 116.19X_2 - 18.81X_1^2 - 19.07 X_1X_2 \quad (3)$$

The $R\%$ profiles over time for each experimental design run are shown in Fig. 6. From Fig. 6, it is possible to observe that even after 120 min, the experiments carried out with the lowest amounts of catalyst (0.1 g L^{-1}) did not achieve significant $R\%$ values, despite the pH value used. For the optimized condition, it is possible to see that the total $R\%$ was reached at 60 min, followed by an experimental condition in the central points, which resulted in a total $R\%$ at 90 min.

Experiments with pristine TiO_2 and CoFe_2O_4 were carried out under the same optimized conditions, i.e., $\text{pH} = 2$ and 1.0 g L^{-1} of catalyst dosage. In addition, the effects of direct photolysis were also investigated by irradiation

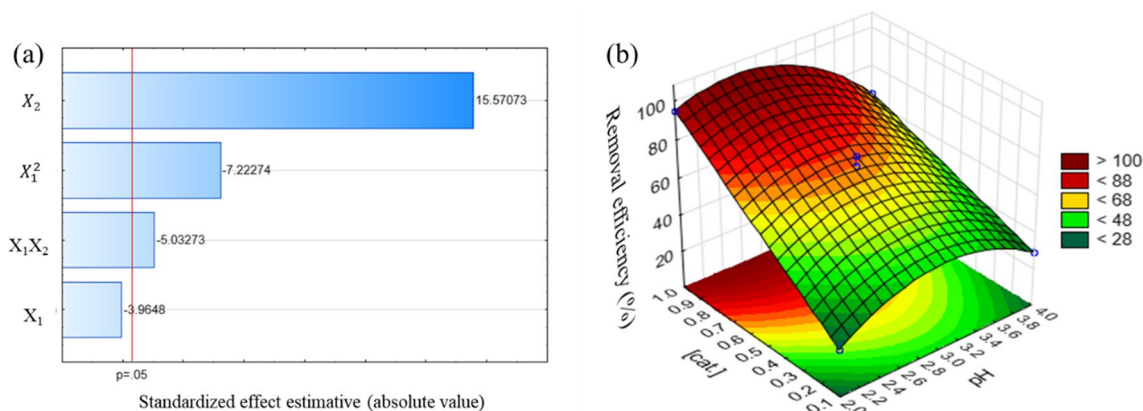


Fig. 5 a Pareto chart for linear and quadratic X_1 and X_2 variables, as well as their interactions. (b) Response surface representing the $R\%$ as a function of pH and catalyst dosage

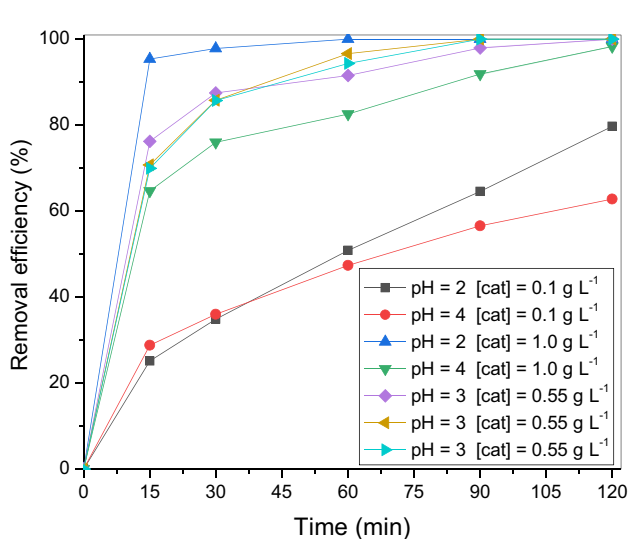


Fig. 6 $R\%$ profiles obtained for each experimental run according to the factorial experimental design

of light only, with the solution at pH 2. The experimental results are shown in Fig. 7. It is possible to observe that the 90Ti catalyst presents superior catalytic activity compared to the other catalysts, reaching an efficiency of 95.39% after 15 min. Its performance was followed by TiO₂, which reached approximately 94% removal after 120 min. For CoFe₂O₄, the maximum removal performance reached was 68% after 120 min.

Moreover, the contribution of direct photolysis by application of light only was limited to approximately 30% at 120 min. According to the $R\%$ profiles obtained, it is possible to infer that the association between TiO₂ and CoFe₂O₄ in one unique semiconductor structure can enhance the photocatalytic activity of the composite over the pristine catalysts. The photocatalytic results are

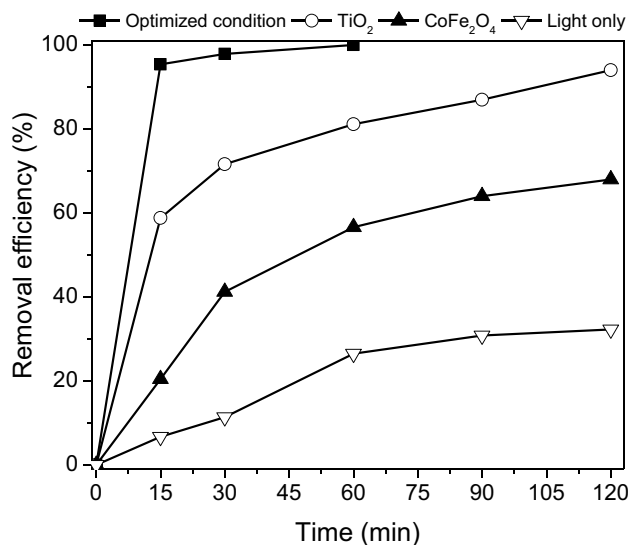


Fig. 7 Comparison of the dye removal efficiencies obtained for the optimized condition (pH=2, catalyst dosage=1.0 g L⁻¹) using 90Ti catalyst against TiO₂ (pH=2, catalyst dosage=1.0 g L⁻¹), CoFe₂O₄ (pH=2, catalyst dosage=1.0 g L⁻¹) and light only

under the characterization results, such as the decrease observed for the band gap of the final composite, especially if compared to pristine TiO₂. In other studies, it has been reported that metal/metal coupling can improve light absorption and lower band gap values of the modified composites, resulting in improvements of approximately 40%, 30%, and 35% for the degradation of methylene blue, rhodamine B, and crystal violet (Revathi et al. 2020). In addition to the optimization of band gap, these effects observed toward the increase for $R\%$ for 90Ti catalyst can also be attributed to the increase in electronic mobility efficiency and decrease in electron-hole recombination factors (Vieira et al. 2022).

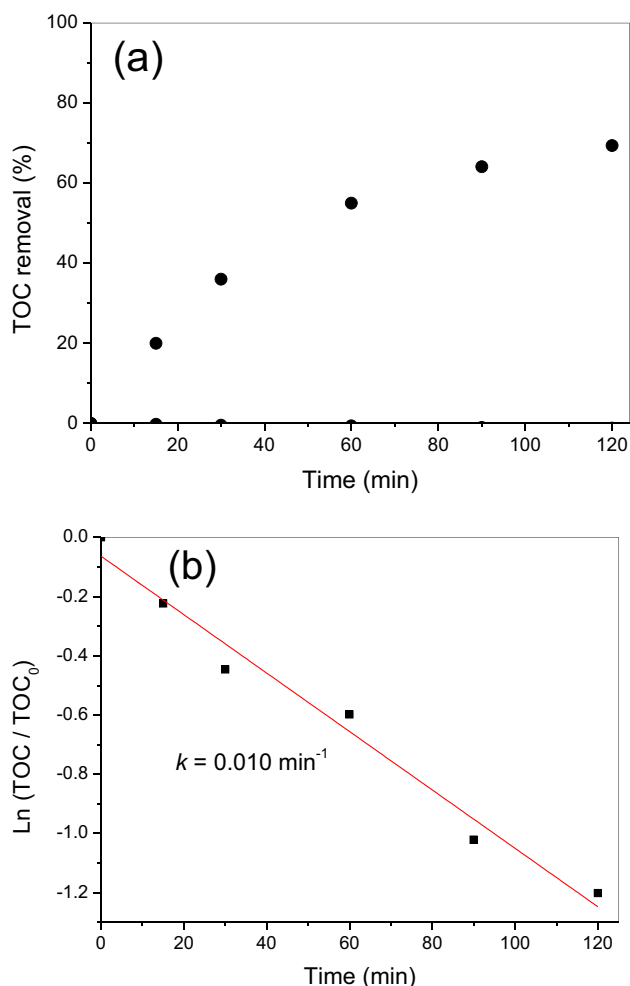


Fig. 8 Concentration variation profile of TOC and (b) first-order kinetic plot for the TOC removal under optimized conditions (pH=2 and catalyst dosage = 1.0 g L⁻¹)

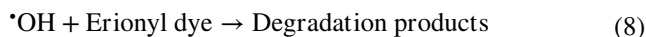
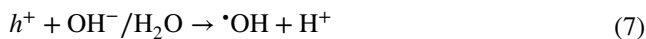
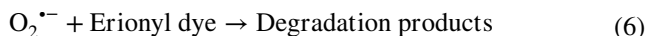
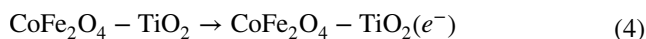
In Fig. 8(a), it is shown the removal profile of TOC during the photocatalytic degradation of dye. As can be seen from Fig. 8(a), satisfactory TOC removal is achieved within 120 min of reaction, around 70%. It is well known that the TOC removal rate is slower than the color removal rate during photodegradation reactions of dyes, needing more time for its complete removal (Aleboye et al. 2008; Anchieta et al. 2014; Anchieta et al. 2015). The rate constant for the TOC removal was estimated by linear regression from the plot of $\ln(\text{TOC}/\text{TOC}_0)$ against time (Fig. 8b), which followed a pseudo-first-order model. The first-order rate constant (k) for the TOC reduction was 0.10 min⁻¹ ($R^2=0.98$). Several studies have shown that the TOC reduction in an aqueous environment involving catalytic reactions for the degradation of organic molecules follows pseudo-first-order kinetics. For instance, the degradation reaction of Reactive Red 141 dye using ZnFe₂O₄ catalyst (Anchieta et al. 2015), degradation of bisphenol A with Ag₃PO₄/Gd₂BiTaO₇ catalyst (Luan et al. 2022), degradation of Amaranth over metal-doped TiO₂ (Divya et al. 2012), and removal of Acid Orange 7 by UV/H₂O₂ process (Aleboye et al. 2008), they all followed pseudo-first-order kinetics.

In Table 2, a summarization of the most relevant photocatalytic parameters of different heterojunctions between TiO₂ and CoFe₂O₄ is presented, which were then applied for the degradation of different organic molecules. From the data compilation, it is possible to conclude that all the heterojunctions show promising results for the degradation of various environmental pollutants. Specifically, it is possible to infer that the 90Ti catalyst prepared in this work presented satisfactory catalytic activity toward Erionyl Red A-3G dye degradation. In addition, the catalyst also shows magnetic behavior (Fig. 9), allowing it to be separated after the reaction is completed by applying a simple external magnetic field, demonstrating its further applicability potential.

Table 2 Comparison among the photocatalytic activities of different heterojunctions between TiO₂ and CoFe₂O₄

| Structure | Molecule | Operating conditions | Efficiency | Reference |
|--------------------------------------------------------------|-------------------|----------------------------------------------------------------------------------------------------------------|----------------|---------------------------|
| TiO ₂ -guanidine-CoFe ₂ O ₄ | Malic acid (MA) | Quartz halogen lamp (150 W); [malic acid] = 0.5 mM; [catalyst] = 2 g L ⁻¹ | 60% in 90 min | (Balu et al. 2011) |
| TiO ₂ /CoFe ₂ O ₄ | Procion Red MX-5B | UV lamp (8 W); [dye] = 10 mg L ⁻¹ ; [catalyst] = 80 mg L ⁻¹ | 90% in 170 min | (Fu et al. 2005) |
| TiO ₂ /CoFe ₂ O ₄ nanofiber | Methylene blue | Hg lamp (300 W); [dye] = 25 mg L ⁻¹ ; [catalyst] = 65 mg L ⁻¹ | 95.87% in 5 h | (Li et al. 2012) |
| CoFe ₂ O ₄ -3D TiO ₂ | Methylene blue | Hg lamp (8 W); [dye] = 5 mg L ⁻¹ ; [catalyst] = 4 g L ⁻¹ | 98.89% in 6 h | (Haw et al. 2016) |
| TiO ₂ /CoFe ₂ O ₄ | Diuron | High-pressure Hg lamp (125 W); [diuron] = 40 mg L ⁻¹ ; pH = 3.0; [catalyst] = 0.5 g L ⁻¹ | 99% in 90 min | (de Oliveira et al. 2020) |
| CoFe ₂ O ₄ /TiO ₂ nanowires | Bromocresol green | High-pressure Hg lamp (100 W); pH = 4.6; [dye] = 8.3 × 10 M; [catalyst] = 0.18 g L ⁻¹ | 60% in 120 min | (Liu et al. 2021) |
| CoFe ₂ O ₄ /TiO ₂ | Erionyl Red A-3G | Hg lamp (250 W); [dye] = 20 mg L ⁻¹ ; pH = 2.0; [catalyst] = 0.55 g L ⁻¹ | 100% in 60 min | This work |

A plausible mechanism for Erionyl Red A-3G degradation could be explained as follows (Haw et al. 2016): when the $\text{CoFe}_2\text{O}_4/\text{TiO}_2$ composite is irradiated by UV light, TiO_2 in composite absorbs more light and thus generates more charges. This causes a transfer of electrons (e^-) from valence band (VB) to conduction band (CB) in TiO_2 , creating holes (h^+) on its VB (Eq. 3). Subsequently, the photogenerated electrons (e^-) migrate from CB of TiO_2 to that of CoFe_2O_4 (Eq. 4), and this promotes an effective e^-/h^+ pair separation, contributing to an inhibition of photogenerated charge recombination, which lead to the improvement of photodegradation activity. The e^- on the CB of CoFe_2O_4 reacts with O_2 to generate $\text{O}_2^{\bullet-}$ radical (Eq. 5), which degrades pollutants (Eq. 6), while h^+ on VB of TiO_2 directly oxidizes organic molecules (Eq. 7), as well as reacts with OH^- or H_2O to generate $\bullet\text{OH}$ radical (Eq. 7), which also acts as an oxidizing species (Eq. 8).



Reusability test

Catalyst reusability is an important parameter that can simultaneously informs the activity and stability of the material. In this work, the catalyst was used for fourth consecutive reuse cycles, under the optimal experimental conditions ($[\text{dye}] = 20 \text{ mg L}^{-1}$; $\text{pH} = 2.0$; $[\text{catalyst}] = 0.55 \text{ g L}^{-1}$) After 60 min of reaction for each cycle, the degradation

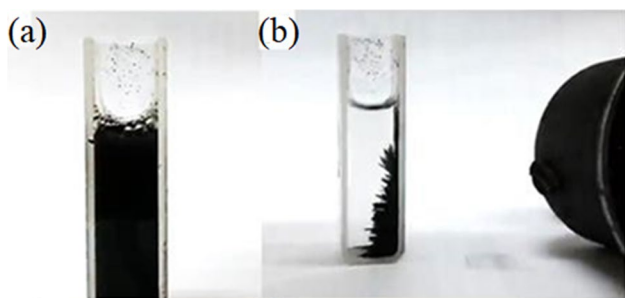


Fig. 9 Images of the nanohybrid particles (a) dispersed in water, and posteriorly (b) subjected to the external magnetic field

efficiencies obtained were 100%, 97.20%, 95.25%, and 90.50% for the 1st, 2nd, 3rd, and 4th cycles, respectively. The results show a photocatalytic potentiality around 90% even after four cycles of reaction, revealing that the catalyst has good efficiency and stability.

Conclusion

The magnetic $\text{CoFe}_2\text{O}_4/\text{TiO}_2$ composite was successfully prepared through a facile solvothermal route. The catalyst presented intrinsic characteristics, such as a smaller band gap value than pristine TiO_2 and magnetic properties. Compared with pristine TiO_2 , $\text{CoFe}_2\text{O}_4/\text{TiO}_2$ catalyst displayed superior photocatalytic efficiency due to its smaller band gap. The nanohybrid catalyst presented remarkable activity toward Erionyl Red A-3G dye degradation, reaching 95.39% color removal after 15 min of reaction and TOC removal of 69.4% after 120 min. These satisfactory values achieved can be attributed to the reduced value of the band gap caused by the heterojunction, as well as the presence of mesoporosity on the surface of the particles. TOC removal kinetics followed the pseudo-first-order model, presenting a rate constant of 0.10 min^{-1} . Furthermore, its magnetic property makes it an easily separable material from an aqueous medium by using a magnet. The catalyst is reusable over four consecutive cycles. In summary, the composite prepared in this work has intrinsic properties that make it a potential catalyst for use in the reduction of organic pollutants in aqueous environments.

Supplementary Information The online version contains supplementary material available at <https://doi.org/10.1007/s11356-023-27762-z>.

Acknowledgements The authors thank the Brazilian funding agencies Coordenação de Aperfeiçoamento de Pessoal de Nível Superior (CAPES) and Conselho Nacional de Desenvolvimento Científico e Tecnológico (CNPq), as well as to the Programa de Recursos Humanos da Agência Nacional de Petróleo, Gás Natural e Biocombustíveis (PRH-ANP), for financial support.

Author contribution Conceptualization: S.B.F. Santos, L.R. Hollanda, E.L. Foletto, O. Chivavone-Filho, and G. L. Dotto; methodology: Y. Vieira, S.B.F. Santos, and L.R. Hollanda; formal analysis and investigation: Y. Vieira, S.B.F. Santos, and L.R. Hollanda; writing—original draft preparation: S.B.F. Santos and L.R. Hollanda; writing—review and editing: E.L. Foletto, O. Chivavone-Filho, and G. L. Dotto; funding acquisition: O. Chivavone-Filho; supervision: E.L. Foletto, O. Chivavone-Filho, and G. L. Dotto. All authors read and approved the final manuscript.

Funding The authors would like to thank CAPES (Coordination for the Improvement of Higher Education Personnel) and CNPq (National Council for Scientific and Technological Development) for the financial support.

Data availability The datasets used and/or analyzed during the current study are available from the corresponding author on reasonable request.

Declarations

Ethical approval Not applicable.

Consent to participate Not applicable.

Consent for publication Not applicable.

Competing interests The authors declare no competing interests.

References

- Abram A, Dražić G (2021) Structural and photocatalytic properties of hydrothermally-prepared boehmite/TiO₂ coatings. *Open Ceram* 7:100153. <https://doi.org/10.1016/J.OCERAM.2021.100153>
- Aleboye A, Olya ME, Aleboye H (2008) Electrical energy determination for an azo dye decolorization and mineralization by UV/H₂O₂ advanced oxidation process. *Chem Eng J* 137:518–524. <https://doi.org/10.1016/j.ccej.2007.05.016>
- Anchieta CG, Cancelier A, Mazutti MA, Jahn SL, Kuhn RC, Gündel A, Chiavone-Filho O, Foletto EL (2014) Effects of solvent diols on the synthesis of ZnFe₂O₄ particles and their use as heterogeneous photo-Fenton catalysts. *Materials* 7:6281–6290. <https://doi.org/10.3390/ma7096281>
- Anchieta CG, Severo EC, Rigo C, Mazutti MA, Kuhn RC, Muller EI, Flores EMM, Moreira RFP, Foletto EL (2015) Rapid and facile preparation of zinc ferrite (ZnFe₂O₄) oxide by microwave-solvothermal technique and its catalytic activity in heterogeneous photo-Fenton reaction. *Mater Chem Phys* 160:141–147. <https://doi.org/10.1016/j.matchemphys.2015.04.016>
- Balu AM, Baruwati B, Serrano E et al (2011) Magnetically separable nanocomposites with photocatalytic activity under visible light for the selective transformation of biomass-derived platform molecules. *Green Chem* 13:2750–2758. <https://doi.org/10.1039/C1GC15692F>
- Ciocarlan RG, Hoeven N, Irtem E et al (2020) Ferrite@TiO₂-nanocomposites as Z-scheme photocatalysts for CO₂ conversion: insight into the correlation of the Co-Zn metal composition and the catalytic activity. *J CO₂ Util* 36:177–186. <https://doi.org/10.1016/J.JCOU.2019.11.012>
- dos Santos JMN, Pereira CR, Pinto LAA et al (2019) Synthesis of a novel CoFe₂O₄/chitosan magnetic composite for fast adsorption of indigotine blue dye. *Carbohydr Polym* 217:6–14. <https://doi.org/10.1016/j.carbpol.2019.04.054>
- Divya N, Bansal A, Jana AK (2012) Photocatalytic activity of transition metal ion doped titania for Amaranth dye degradation. *Mater Sci Forum* 712:85–104. <https://doi.org/10.4028/www.scientific.net/MSF.712.85>
- de Oliveira JS, da Costa Halmenschlager F, Jahn SL, Foletto EL (2019) Síntese de CoFe₂O₄ sobre os suportes MgAl₂O₄ e ZSM-5 para uso na degradação de poluente orgânico pelo processo foto-Fenton heterogêneo sob irradiação visível e solar. *Matéria (Rio Janeiro)* 24. <https://doi.org/10.1590/S1517-707620190004.0823>
- de Oliveira PL, Lima NS, de Melo Costa ACF et al (2020) Obtaining TiO₂:CoFe₂O₄ nanocatalyst by Pechini method for diuron degradation and mineralization. *Ceram Int* 46:9421–9435. <https://doi.org/10.1016/J.CERAMINT.2019.12.203>
- Fu W, Yang H, Li M et al (2005) Anatase TiO₂ nanolayer coating on cobalt ferrite nanoparticles for magnetic photocatalyst. *Mater Lett* 59:3530–3534. <https://doi.org/10.1016/J.MATLET.2005.06.071>
- Fuziki MEK, Brackmann R, Dias DT et al (2021) Effects of synthesis parameters on the properties and photocatalytic activity of the magnetic catalyst TiO₂/CoFe₂O₄ applied to selenium photoreduction. *J Water Process Eng* 42:102163. <https://doi.org/10.1016/J.JWPE.2021.102163>
- Hafeez HY, Lakhera SK, Narayanan N et al (2019) Correction to "environmentally sustainable synthesis of CoFe₂O₄-TiO₂/rGO ternary photocatalyst: a highly efficient and stable photocatalyst for high production of hydrogen (solar fuel)". *ACS Omega* 4:2980. <https://doi.org/10.1021/ACSOMEGA.9B00169>
- Haw C, Chiu W, Abdul Rahman S et al (2016) The design of new magnetic-photocatalyst nanocomposites (CoFe₂O₄-TiO₂) as smart nanomaterials for recyclable-photocatalysis applications. *New J Chem* 40:1124–1136. <https://doi.org/10.1039/C5NJ02496J>
- Heydari M, Gharagozlou M, Ghahari M, Sadjadi S (2021) Synthesis and characterization of CoFe₂O₄@TiO₂@HKUST-1 as a novel metal-organic framework nanocomposite. *Inorg Chem Commun* 130:108693. <https://doi.org/10.1016/J.INOCHE.2021.108693>
- Hollanda LR, Santos SBF, Faustino JGAA et al (2021) Oil field-produced water treatment: characterization, photochemical systems, and combined processes. *Environ Sci Pollut Res* 28:52744–52763. <https://doi.org/10.1007/S11356-021-16222-1>
- Lazarotto JS, de Lima BV, Silvestri S, Foletto EL (2020) Conversion of spent coffee grounds to biochar as promising TiO₂ support for effective degradation of diclofenac in water. *Appl Organomet Chem* 34:e6001. <https://doi.org/10.1002/AOC.6001>
- Li CJ, Wang JN, Wang B et al (2012) A novel magnetically separable TiO₂/CoFe₂O₄ nanofiber with high photocatalytic activity under UV-vis light. *Mater Res Bull* 47:333–337. <https://doi.org/10.1016/J.MATERRESBULL.2011.11.012>
- Liu Z, Wang N, Ma L et al (2021) Elaboration and photocatalytic properties of CoFe₂O₄/TiO₂ composite nanowires with the side-by-side structure. *Mater Res Bull* 141:111354. <https://doi.org/10.1016/J.MATERRESBULL.2021.111354>
- Luan J, Wei Z, Niu B, Yang G, Huang C, Ma B, Liu W (2022) Synthesis, property characterization and photocatalytic activity of the Ag₃PO₄/Gd₂BiTaO₇ heterojunction catalyst under visible light irradiation. *Catalysts* 12:22. <https://doi.org/10.3390/catal12010022>
- Mapossa AB, Mhike W, Adalima JL et al (2021) Removal of organic dyes from water and wastewater using magnetic ferrite-based titanium oxide and zinc oxide nanocomposites: a review. *Catal* 11(12):1543. <https://doi.org/10.3390/CATAL11121543>
- Mourão HAJL, Malagutti AR, Ribeiro C (2010) Synthesis of TiO₂-coated CoFe₂O₄ photocatalysts applied to the photodegradation of atrazine and rhodamine B in water. *Appl Catal Gen* 382:284–292. <https://doi.org/10.1016/J.APCATA.2010.05.007>
- Nabi G, Raza W, Kamran MA et al (2020) Role of cerium-doping in CoFe₂O₄ electrodes for high performance supercapacitors. *J Energy Storage* 29:101452. <https://doi.org/10.1016/J.EST.2020.101452>
- Oliveira JS, Mazutti MA, Urquieta-Gonzalez EA, Foletto EL, Jahn SL (2016) Preparation of mesoporous Fe₂O₃-supported ZSM-5 zeolites by carbon-templating and their evaluation as photo-Fenton catalysts to degrade organic pollutant. *Mater Res* 19:1399–1406. <https://doi.org/10.1590/1980-5373-MR-2016-0367>
- Oliveira JS, Brondani M, Mallmann ES, Jahn SL, Foletto EL, Silvestri S (2018) Preparation of highly efficient CoFe₂O₄/Zn₂SnO₄ composite photocatalyst for the degradation of rhodamine B dye from aqueous solution. *Water Air Soil Pollut* 229:1–9. <https://doi.org/10.1007/s11270-018-4038-0>
- Oliveria FR, De Oliveira DAJ, Steffens F et al (2017) Dyeing of cotton and polyester blended fabric previously cationized with synthetic and natural polyelectrolytes. *Procedia Eng* 200:309–316. <https://doi.org/10.1016/J.PROENG.2017.07.044>
- Osege EO, Ofomaja AE (2018) Study on light emission diode/carbon modified TiO₂ system for tetracycline hydrochloride degradation. *J Photochem Photobiol A Chem* 360:242–248. <https://doi.org/10.1016/j.jphotochem.2018.04.048>

- Parhizkar J, Habibi MH (2018) Mosavian SY (2018) Synthesis and characterization of nano CoFe_2O_4 prepared by sol-gel auto-combustion with ultrasonic irradiation and evaluation of photocatalytic removal and degradation kinetic of Reactive Red 195. *Silicon* 112(11):1119–1129. <https://doi.org/10.1007/S12633-018-9922-0>
- Pérez-Osorio G, Hernández-Aldana F, Hernández JCM, Arriola-Morales J, Castillo-Morales M, Gutiérrez-Martin SN, Gutiérrez-Arias JM (2019) Photodegradation of Erionyl dye in aqueous medium by sunlight and palladium catalysts. *Rev Mex Ing Quim* 8:1027–1035. <https://doi.org/10.24275/uam/izt/dcbi/revmexingquim/2019v18n3/Perez>
- Revathi J, Abel MJ, Archana V et al (2020) Synthesis and characterization of CoFe_2O_4 and Ni-doped CoFe_2O_4 nanoparticles by chemical Co-precipitation technique for photodegradation of organic dyestuffs under direct sunlight. *Phys B Condens Matter* 587:412136. <https://doi.org/10.1016/J.PHYSB.2020.412136>
- Rossatto DL, Netto MS, Jahn SL et al (2020) Highly efficient adsorption performance of a novel magnetic geopolymer/ Fe_3O_4 composite towards removal of aqueous acid green 16 dye. *J Environ Chem Eng*. <https://doi.org/10.1016/j.jece.2020.103804>
- Krishna S, Sathishkumar P, Pugazhenthiran N et al (2020) Heterogeneous sonocatalytic activation of peroxomonosulphate in the presence of $\text{CoFe}_2\text{O}_4/\text{TiO}_2$ nanocatalysts for the degradation of Acid Blue 113 in an aqueous environment. *J Environ Chem Eng* 8:104024. <https://doi.org/10.1016/J.JECE.2020.104024>
- Sathishkumar P, Mangalaraja RV, Anandan S, Ashokkumar M (2013) $\text{CoFe}_2\text{O}_4/\text{TiO}_2$ nanocatalysts for the photocatalytic degradation of Reactive Red 120 in aqueous solutions in the presence and absence of electron acceptors. *Chem Eng J* 220:302–310. <https://doi.org/10.1016/J.CEJ.2013.01.036>
- Silva CG, Wang W, Faria JL (2006) Photocatalytic and photochemical degradation of mono-, di- and tri-azo dyes in aqueous solution under UV irradiation. *J Photochem Photobiol A: Chem* 181:314–324. <https://doi.org/10.1016/j.jphotochem.2005.12.013>
- Silvestri S, Foletto EL (2017) Preparation and characterization of $\text{Fe}_2\text{O}_3/\text{TiO}_2/\text{clay}$ plates and their use as photocatalysts. *Ceram Int* 43:14057–14062. <https://doi.org/10.1016/j.ceramint.2017.07.140>
- Silvestri S, Stefanello N, Sulkovski AA, Foletto EL (2020) Preparation of TiO_2 supported on MDF biochar for simultaneous removal of methylene blue by adsorption and photocatalysis. *J Chem Technol Biotechnol* 9:2723–2729. <https://doi.org/10.1002/jctb.6279>
- Sing KSW, Everett DH, Haul R et al (1985) Reporting physisorption data for gas/solid systems-with special reference to the determination of surface area and porosity. *Pure Appl Chem* 57:603–619. <https://doi.org/10.1351/pac198557040603>
- Stefan M, Leostean C, Toloman D et al (2021) New emerging magnetic, optical and photocatalytic properties of Tb doped TiO_2 interfaced with CoFe_2O_4 nanoparticles. *Appl Surf Sci* 570:151172. <https://doi.org/10.1016/J.APSUSC.2021.151172>
- Sun Q, Wu S, Li K et al (2020) The favourable synergistic operation of photocatalysis and catalytic oxygen reduction reaction by a novel heterogeneous $\text{CoFe}_2\text{O}_4\text{-TiO}_2$ nanocomposite. *Appl Surf Sci* 516:146142. <https://doi.org/10.1016/J.APSUSC.2020.146142>
- Thommes M, Kaneko K, Neimark AV et al (2015) Physisorption of gases, with special reference to the evaluation of surface area and pore size distribution (IUPAC Technical Report). *Pure Appl Chem* 87:1051–1069. <https://doi.org/10.1515/PAC-2014-1117/PDF>
- Van TC, La DD, Thi Hoai PN et al (2021) New TiO_2 -doped Cu–Mg spinel-ferrite-based photocatalyst for degrading highly toxic rhodamine B dye in wastewater. *J Hazard Mater* 420:126636. <https://doi.org/10.1016/J.JHAZMAT.2021.126636>
- Vaiano V, Sannino D, Sacco O (2020) The use of nanocatalysts (and nanoparticles) for water and wastewater treatment by means of advanced oxidation processes. *Nanotechnol Beverage Ind Fundam Appl* 241–264. <https://doi.org/10.1016/B978-0-12-819941-1.00009-2>
- Vieira Y, da Boit MK, Ribeiro TH et al (2022) Photo-assisted degradation of organic pollutant by CuFeS_2 powder in RGB-LED reactors: a comprehensive study of band gap values and the relation between wavelength and electron-hole recombination. *Adv Powder Technol* 33:103368. <https://doi.org/10.1016/J.APT.2021.11.020>
- Vieira Y, Leichtweis J, Foletto EL, Silvestri S (2019) Reactive oxygen species-induced heterogeneous photocatalytic degradation of organic pollutant rhodamine B by copper and zinc aluminate spinels. *J Chem Technol Biotechnol*. <https://doi.org/10.1002/jctb.6267>
- Vieira Y, Silvestri S, Leichtweis J et al (2020) New insights into the mechanism of heterogeneous activation of nano-magnetite by microwave irradiation for use as Fenton catalyst. *J Environ Chem Eng* 8:103787. <https://doi.org/10.1016/j.jece.2020.103787>
- Vlazan P, Stoia M (2018) Structural and magnetic properties of CoFe_2O_4 nanopowders, prepared using a modified Pechini method. *Ceram Int* 44:530–536. <https://doi.org/10.1016/J.CERAMINT.2017.09.207>
- Wang N, Sun X, Zhao Q, Wang P (2021) Treatment of polymer-flooding wastewater by a modified coal fly ash-catalysed Fenton-like process with microwave pre-enhancement: system parameters, kinetics, and proposed mechanism. *Chem Eng J* 406:126734. <https://doi.org/10.1016/J.CEJ.2020.126734>
- Yaseen DA, Scholz M (2019) Textile dye wastewater characteristics and constituents of synthetic effluents: a critical review *Int J Environ Sci Technol* 16(2):1193–1226. <https://doi.org/10.1007/s13762-018-2130-z>
- Zayani G, Bousselmi L, Pichat P, Mhenni F, Ghrabi A (2006) Photocatalytic degradation of four textile azo dyes in aqueous TiO_2 suspensions: practical outcomes and revisited pathways. *J Adv Oxid Technol* 9:65–78. <https://doi.org/10.1515/jaots-2006-0110>

Publisher's note Springer Nature remains neutral with regard to jurisdictional claims in published maps and institutional affiliations.

Springer Nature or its licensor (e.g. a society or other partner) holds exclusive rights to this article under a publishing agreement with the author(s) or other rightsholder(s); author self-archiving of the accepted manuscript version of this article is solely governed by the terms of such publishing agreement and applicable law.